Study on the Synthesis and Properties of Metal-organic Complex Containing Samarium①

DING Yi-Fan[a, b] LI Fei[b] YANG Jin-Xia[b]
QIN Ye-Yan[b] YAO Yuan-Gen[a, b②]

[a] (*College of Chemistry, Fuzhou University, Fuzhou* 350116, *China*)

[b] (*Key Laboratory of Coal to Ethylene Glycol and Its Related Technology, Fujian Institute of Research on the Structure of Matter, Chinese Academy of Sciences, Fuzhou* 350002, *China*)

ABSTRACT A new rare earth organic complex with a double interleaved structure, namely $[Sm(BDC)_{1.5}(DMF)(H_2O)]_n$ (H_2BDC = 1,4-benzenedicarboxylic acid, DMF = N,N´-dimethyl formamide) was synthesized. The crystal structure is of triclinic, space group $P\bar{1}$ with a = 8.6343(6), b = 10.1470(5), c = 11.2073(6) Å, α = 65.495(5), β = 71.626(5), γ = 78.130(5) °, V = 844.70(9) Å^3, $C_{15}H_{15}NO_8Sm$, M_r = 487.64, Z = 2, D_c = 1.917 g/cm^3, F(000) = 476, μ = 3.519 mm^{-1}, R = 0.0380 and wR = 0.0864 for 3504 observed reflections ($I > 2\sigma(I)$). The structure has been determined by single-crystal X-ray diffraction analyses and displays a 2-fold interpenetrated 3D network with the classical **pcu** topology. The compound was analyzed by X-ray powder, infrared spectroscopy, thermogravimetric analysis and fluorescent spectroscopy. The fluorescent property makes it a good candidate for photoactive materials.

Keywords: samarium, fluorescent, earth organic compound; DOI: 10.14102/j.cnki.0254–5861.2011–3076

1 INTRODUCTION

Metal-organic framework materials have become a hot spot in the field of materials chemistry due to their good structural tailorability and easy functionalization[1-3]. At present, people have been able to use the crystal engineering of coordination polymers to control the structures of coordination polymers to a certain extent, and at the same time, they can also select functional central metal ions and organic ligands with functional groups to give the target coordination polymers. With functions such as optical, electrical, magnetic, hand-shaped resolution, catalysis, ferroelectricity, and second-order nonlinear optical properties, aromatic polycarboxylate acids have been widely studied in the coordination field due to the diversity of their carboxyl group coordination[4-11]. Rigid carboxylic acid ligands containing oxygen atoms are one of the most common ligands for preparing functional metal compounds. Among them, terephthalic acid has two 180 ° carboxyl groups and one conjugated benzene ring. It can build a very characteristic structure with transition metals or rare earths[12-14].

The excitation and luminescence of rare earth elements are caused by the transition of rare earth 4*f* electrons between different energy levels. There are *f-f* transitions between different energy levels in the *f* configuration, and *f-d* transitions between the *f* and *d* configurations. The energy difference between the excited and ground states of 4*f* electrons in different rare earth ions is different, so their luminescence properties are very different[15-19]. In recent years, the rare earth complexes of dibasic aromatic acid have been continuously synthesized. Its luminous performance has also been studied in depth. With rare earth elements and terephthalic acid as the basic building units, people use solvothermal synthesis, reverse microemulsion method, etc. successively obtained a series of coordination polymers with the same crystal structure[20-26]. The fluorescence intensity of the Sm^{3+} ions is relatively weak,

Received 25 December 2020; accepted 26 February 2021 (**CCDC 1988467**)

① This research was supported by the NSF of China (21703247) and the Science Foundation of Fujian Province (2018J05029, 2019J05156, 2019H0053)

② Corresponding author. E-mail: yyg@fjirasm.ac.cn

and there is not much research on it. The reason is that no suitable ligands for Sm^{3+} compoundes to emit light have yet been developed. However, the red light emitted by the complex with samarium metal as the core ion is the best match with the spectral properties required for plant photosynthesis. Because the characteristic coordination atom of rare earth ion is oxygen, it can react with many oxygen-containing ligands.

Based on above consideration, this paper utilized Sm^{3+} as the central ion and terephthalic acid as the rigid ligand to synthesize a novel rare earth organic compound, namely $[Sm(BDC)_{1.5}(DMF)(H_2O)]_n$ (H_2BDC = 1,4-benzenedicarboxylic acid, DMF = N,N′-dimethylformamide). Furthermore, luminescent property of this complex has also been investigated in detail.

2 EXPERIMENTAL

2. 1 Materials and methods

Common reagents were purchased from general commercial channels and used without further purification. All compounds were synthesized under solvothermal conditions. Elemental analyses (C, H, N) were measured on a Vario El-Cube elemental analyser. The powder X-ray diffraction (PXRD) data were collected on a Rigaku MiniFlex II diffractometer by Cu$K\alpha$ radiation. Simulated PXRD patterns were derived from the Mercury Version 3.10.2 software using the X-ray single crystal diffraction data. Thermo-gravimetric analyses (TGA) were carried out on a NETSCHZ STA-449C thermal analyzer under a nitrogen atmosphere and at a rate of 10 ℃ min^{-1}, starting from room temperature. Emission, excitation spectra were measured on an Edinburgh FLS980 fluorescence spectrophotometer in the solid state.

2. 2 Synthesis of $[Sm(BCD)_{1.5}(DMF)(H_2O)]_n$ (1)

Reactions of $Sm(NO_3)_3$ $6H_2O$ (0.2 mol), H_2BDC (0.2 mol) in the DMF/H_2O media (15 mL v/v = 2:1) under ultrasonic treatment 30 min. Then, the resultant colorless solution was reacted in a 100 ℃ oven for 3days to give colorless crystals of 1 in 30% yield (based on $Sm(NO_3)_3$ $6H_2O$). Elemental analyses calcd. for $C_{15}H_{15}NO_8$ Sm (291.04): C, 36.95; H, 3.10; N, 2.87%. Found: C, 37.32; H, 3.1; N, 2.35%.

2. 3 Single crystal X-ray diffraction determination

X-ray diffraction data were collected on a Rigaku Oxford SuperNova Single Source diffractometer with an Eos detector and a Mo$K\alpha$ radiation radiation (λ = 0.71073 Å). CrysAlisPro Agilent Technologies software was used for collecting the frames of data, indexing the reflections, determining the lattice constants, absorption correction, and data reduction[27]. The structures were solved by the direct methods, successive Fourier difference syntheses, and refined by the full-matrix least-squares method on F^2 (SHELXTL-2014)[28]. All non-hydrogen atoms are refined with anisotropic thermal parameters. Hydrogen atoms bonded to the carbon atoms were assigned to calculated positions. The water and hydroxyl hydrogen atoms could not be located. The selected bond lengths and angles of **1** are listed in are listed in Table 1.

Table 1. Selected Bond Lengths and Bond Angles for 1

Bond	Dist.	Bond	Dist.	Bond	Dist.
Sm(1)–O(7)	2.389(4)	Sm(1)–O(6)^a	2.446(4)	Sm(1)–O(2)	2.485(3)
Sm(1)–O(1w)	2.424(3)	Sm(1)–O(1)	2.454(4)	Sm(1)–O(4)	2.521(3)
Sm(1)–O(3)	2.433(3)	Sm(1)–O(5)	2.455(3)		
Bond	(°)	Bond	(°)	Bond	(°)
O(7)–Sm(1)–O(1w)	76.41(14)	O(7)–Sm(1)–O(5)	93.99(12)	O(5)–Sm(1)–O(2)	72.74(11)
O(7)–Sm(1)–O(3)	86.86(13)	O(1w)–Sm(1)–O(5)	75.88(12)	O(7)–Sm(1)–O(4)	76.17(13)
O(1w)–Sm(1)–O(3)	131.56(12)	O(3)–Sm(1)–O(5)	151.44(12)	O(1w)–Sm(1)–O(4)	79.01(12)
O(7)–Sm(1)–O(6)^a	148.82(14)	O(6)^a–Sm(1)–O(5)	114.58(11)	O(3)–Sm(1)–O(4)	52.76(11)
O(1w)–Sm(1)–O(6)^a	97.82(14)	O(1)–Sm(1)–O(5)	77.54(11)	O(6)^a–Sm(1)–O(4)	72.65(13)
O(3)–Sm(1)–O(6)^a	74.07(13)	O(7)–Sm(1)–O(2)	126.52(13)	O(1)–Sm(1)–O(4)	120.48(12)
O(7)–Sm(1)–O(1)	73.85(13)	O(1w)–Sm(1)–O(2)	141.85(12)	O(5)–Sm(1)–O(4)	154.58(11)
O(1w)–Sm(1)–O(1)	138.17(13)	O(3)–Sm(1)–O(2)	83.85(11)	O(2)–Sm(1)–O(4)	131.89(11)
O(3)–Sm(1)–O(1)	75.30(12)	O(6)^a–Sm(1)–O(2)	76.52(13)	O(7)–Sm(1)–O(5)^a	147.51(12)
O(6)^a–Sm(1)–O(1)	122.58(13)	O(1)–Sm(1)–O(2)	52.83(11)	O(1w)–Sm(1)–O(5)^a	73.88(12)
O(3)–Sm(1)–O(5)^a	123.04(11)	O(6)^a–Sm(1)–O(5)^a	50.15(10)	O(1)–Sm(1)–O(5)^a	122.49(11)
O(5)–Sm(1)–O(5)^a	66.28(12)	O(2)–Sm(1)–O(5)^a	73.97(11)	O(4)–Sm(1)–O(5)^a	110.27(11)

a = 1−*x*, −*y*, 2−*z*

3 RESULTS AND DISCUSSION

3. 1 Synthesis and characterization

It can be seen from Fig. 1a, the smallest asymmetric unit of complex **1** contains one Sm^{3+} cation, three half BDC^{2-} ligands, one coordinated water molecule, and one coordinated DMF molecule. The Sm^{3+} center is nine-coordinated in a twisted double-hat pentagonal biconical geometry by seven O atoms from four BDC^{2-} ligands, one O atom from DMF, and one O atom from water molecule, and presents a twisted double-hat pentagonal biconical geometry. For convenience, the BDC^{2-} ligands containing O(1), O(3), and O(5) are designated as BDC-1, BDC-2, and BDC-3, respectively. The Sm–O bond lengths of Sm coordinated with the oxygen atoms are between 2.389(4)~2.521(3) Å, and these M–O bond lengths are all within the normal Sm–O bond length range[16].

As shown in Fig. 1b, both BDC-1 and BDC-2 ligands adopt a μ_2-η^1:η^1:η^1:η^1 chelating mode and the BDC-3 ligands are in a μ_4-η^1:η^2:η^1:η^2 chelating-bridging fashion.

Two adjacent Sm^{3+} cations are linked by two bridging carboxylate groups to yield a dinuclear $[Sm_2(CO_2)_2]$ cluster with a Sm ··Sm separation of 4.33 Å. Each $[Sm_2(CO_2)_2]$ cluster links to its neighbouring clusters by the BDC-2 and BDC-3 ligands, resulting in a 2D layer (Fig. 1b). Furthermore, these 2D layers are further pillared by the BDC-1 ligands to form a 3D pillar-layered framework (Fig. 1c). From the topological view, the $[Sm_2(CO_2)_2]$ cluster can be simplified as a six-connected node (Fig. 1d), the BDC^{2-} ligands are taken as linkers, and the 3D structure can be classified as a classical **pcu** architecture (Fig. 1e). Along the *b* axis, the large hexagonal channels within a single 3D network allow for the interpenetration of an identical net, which directly leads to the formation of a 2-fold interpenetrating final framework (Fig. 1f). In addition, the DMF and water molecules coordinate the Sm^{3+} cations to finish the coordination sphere of the metal ions and give a more stabilized 3D structure (Fig. 2).

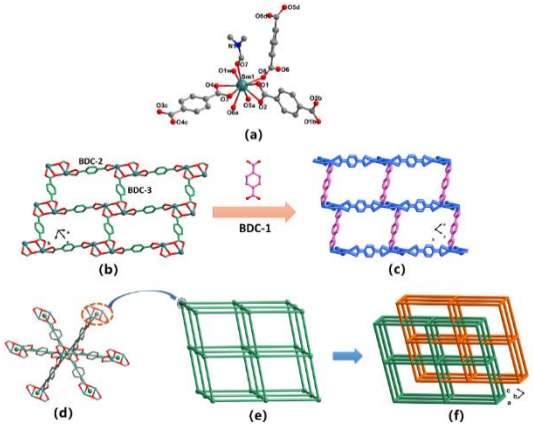

Fig. 1. (a) Coordination environment of Sm1 in complex 1 (symmetry codes: a = 1−*x*, −*y*, 2−*z*; b = 2−*x*, −*y*, 1−*z*; c = −*x*, 1−*y*, 1−*z*; d = 1−*x*, −1−*y*, 2−*z*). (b) The 2D sheet formed by $[Sm_2(CO_2)_2]$ clusters and BDC ligands. framework of 1. (c) View of the single 3D open (d) Perspective view of the six-connected node in 1. (e) Schematic view of the pcu topology. (f) Schematic representation of the 2-fold interpenetrating networks

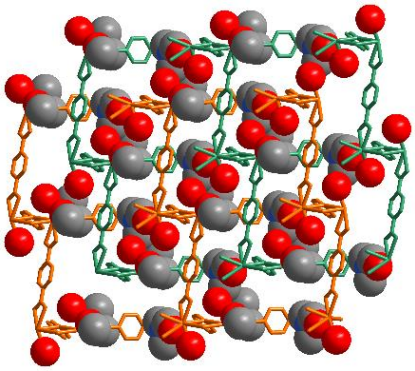

Fig. 2. 2-fold interpenetrated 3D framework with water molecules and DMF filled in the channels in 1 (The 2-fold interpenetrated networks are presented in different colors for clarity)

3. 2 XRD and TG analysis

In order to confirm the phase purity of complex **1**, the powder X-ray diffraction (PXRD) experiments were carried out. From the Fig. 3, it can be seen that the X-ray diffraction peaks of the complex obtained in the experiment are basically consistent with the simulated spectrum, which indicates that the purity of complex **1** is high and the related characterization is reliable.

As can be seen from Fig. 4, complex **1** can exist stably in the air and maintain a stable crystal state at room temperature which makes it potential candidate for practical applications. In order to explore the thermal stability of complex **1**, we conducted thermo-gravimetric analysis in the temperature range of 30~800 ℃. The initial mass loss of complex **1** is 141~252 °C. This weight loss process is attributed to the departure of coordinated water molecules and DMF (theoretical weight loss is 18.1%, actual weight loss is 18.5%). Thereafter, a stable platform was maintained between 252~552 °C, which indicated that the framework of the complex was stable at this temperature. The second weight loss occurs in the range of 552~667 °C, corresponding to the decomposition of BDC ligands. The entire framework of the complex collapses, remaining participants Sm_2O_3.

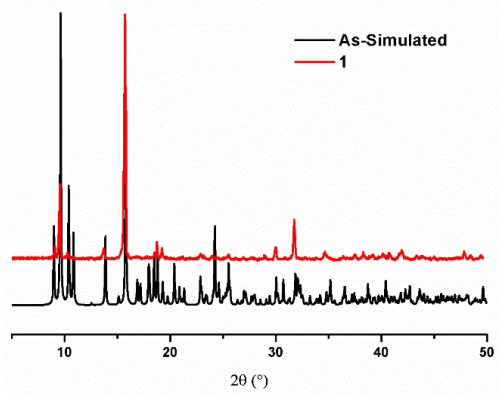

Fig. 3. Experimental and simulated XRD pattern of complex 1

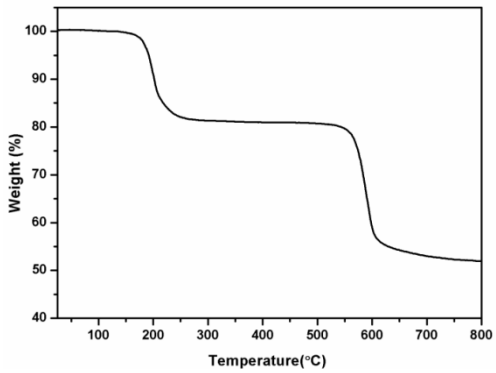

Fig. 4. TGA curve of complex 1

3. 3 Solid state fluorescence performance

Luminescent rare earth organic frameworks have received great attention due to their potential applications in chemical sensors, photochemistry and rare earth light transfer agents. In this work, we studied the solid-state luminescence of ligands and complex **1** at room temperature. Performance, as a result, the complex shows strong fluorescence. The solid-state excitation and emission spectra of H_2BDC ligand at room temperature. H_2BDC is excited at 332 nm. H_2BDC shows a broad band peak at 385 nm, which may be due to $\pi^*\rightarrow\pi$ or $\pi^*\rightarrow n$ electronic transition (LLCT)[29]. Complex **1** solid state excitation and emission spectra were performed at room temperature. The excitation spectrum is obtained by monitoring the strongest emission wavelength of Sm^{3+} at 643 nm. The excitation spectrum has narrow and sharp excitation peaks in several other places, which are attributed to the characteristic excitation spectrum of Sm^{3+} ions. The indirect excitation of the ligand in complex **1** is dominant, indicating that the sensitization of Sm^{3+} luminescence is mainly through the indirect energy transfer process from the ligand to the Sm^{3+} ion. When excited at 297 nm, the emission spectrum of complex **1** shows the characteristic spectral lines of Sm^{3+}, showing characteristic emission bands of $^4G_{5/2}$ to $^6H_{5/2,}$ $^4G_{5/2}$ to $^6H_{7/2,}$ $^4G_{5/2}$ to $^6H_{9/2,}$ $^4G_{5/2}$ to $^6H_{11/2}$ at 560, 595, 640 nm and 702 nm, respectively. In addition to the characteristic emission band of Sm^{3+} ion, complex **1** also shows the emission band in the blue region, which is due to the energy conversion within the ligand, which indicates that the energy conversion from the ligand to Sm^{3+} is not very effective. (Fig. 5) It can be seen from Fig. 5 that the ligand is in the orange region and the compound is in the blue region.

Obviously, the ligand has no effect on the luminescence of the complex **1**. The complex has fluorescence emission peaks around 560, 595, 641 and 703 nm, which correspond to the $^4G_{5/2}$ to $^6H_{5/2,}$ $^4G_{5/2}$ to $^6H_{7/2,}$ $^4G_{5/2}$ to $^6H_{9/2,}$ $^4G_{5/2}$ to $^6H_{11/2}$ transitions of Sm^{3+}, respectively. The emission spectrum of the complex is the characteristic spectrum of Sm(Ⅲ) perturbed by the ligand.

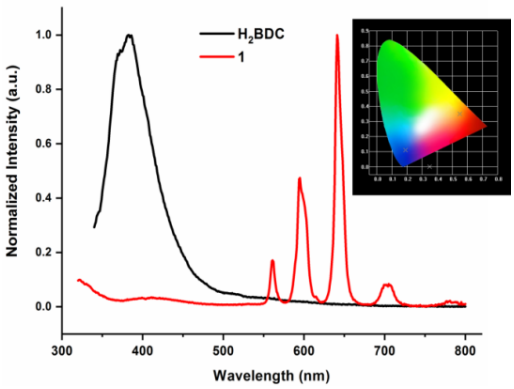

Fig. 5. Emission spectrum of H_2BCD at λ_{ex}= 332 nm and Emission spectrum of 1 at λ_{ex} = 297 nm. Inset: photograph of its CIE color coordinates

4 CONCLUSION

This paper uses terephthalic acid as the ligand and cheap rare earth Sm as the central metal to synthesize a double-interleaved 3D structure, and analyze its structure and performance. Furthermore, the photoluminescence measurements reveal that complex **1** is a good candidate for photoactive materials, owing to their strong luminescent emissions.

REFERENCES

(1) Armelao, L.; Quici, S.; Barigelletti, F.; Accorsi, G.; Bottaro, G.; Cavazzini M.; Tondello, E. Design of luminescent lanthanide complexes: from molecules to highly efficient photo-emitting materials. *Coord. Chem. Rev.* **2010**, 254, 487–505.

(2) Feng, J.; Zhang, H. J. Hybrid materials based on lanthanide organic complexes: a review. *Chem. Soc. Rev*. **2013**, 42, 387–410.

(3) Lu, W. G.; Wei, Z. W.; Gu, Z. Y.; Liu, T. F.; Park, J.; Park, J.; Tian, J.; Zhang, M. W.; Zhang, Q.; Gentle, T.； Bosch, M.; Zhou, H. C. Tuning the structure and function of metal-organic frameworks via linker design. *Chem. Soc. Rev.* **2014**, 43, 5561–5593.

(4) Deslandes, S.; Galaup, C.; Poole, R.; Mestre-Voegtle, B.; Soldevila, S.; Leygue, N.; Bazin, H.; Lamarque，L.; Picard, C. Synthesis and optical properties of macrocyclic lanthanide(III) chelates as new reagents for luminescent biolabeling. *Org. Biomol. Chem*. **2012**, 10, 8509–8523.

(5) Armelao, L.; Bottaro, G.; Quici, S.; Cavazzini, M.; Scalera, C.; Accorsi, G. Synthesis and photophysical characterization of highly luminescent silica films doped with substituted 2-hydro-xyphthalamide (IAM) terbium complexes. *Dalton Trans*. **2011**, 40, 11530–11538.

(6) Bourdolle, A.; Allali, M.; Mulatier, J. C.; Le Guennic, B.; Zwier, J. M.; Baldeck, P. L.; Bunzli, J. C. G.; Andraud, C.; Lamarque, L.; Maury, O. Modulating the photophysical properties of azamacrocyclic europium complexes with charge-transfer antenna chromophores. *Inorg. Chem.* **2011**, 50, 4987–4999.

(7) Yang, J.; Song, S. Y.; Ma, J. F.; Liu Y. Y.; Yu, Z. T. Syntheses, structures, photoluminescence, and gas adsorption of rare earth-organic frameworks based on a flexible tricarboxylate. *Cryst. Growth Des.* **2011**, 11, 5469–5474.

(8) Zhang, W. X.; Yang, Y. Y.; Zai, S. B.; Ng, S. W.; Chen, X. M. Syntheses, structures and magnetic properties of dinuclear copper(II)-lanthanide(III) complexes bridged by 2-hydroxy-methyl-1-methylimidazole. *Eur. J. Inorg. Chem*. **2008**, 5, 679–685.

(9) Zheng, Y. H.; Lin, J. T.; Wang, Q. M. Emissions and photocatalytic selectivity of $SrWO_4$:Ln^{3+} (Eu^{3+}, Tb^{3+}, Sm^{3+} and Dy^{3+}) prepared by a supersonic microwave co-assistance method. *Photochem. Photobiol. Sci*. **2012**, 11, 1567–1574.

(10) Tan, C. L.; Wang, Q. M. Reversible terbium luminescent polyelectrolyte hydrogels for detection of $H_2PO_4^-$ and HSO_4^- in water. *Inorg. Chem.* **2011**, 50, 2953–2956.

(11) Wang, Q. M.; Tan, C. L.; Cai, W. S. A targetable fluorescent sensor for hypochlorite based on a luminescent europium complex loaded carbon nanotube. *Analyst*. **2012**, 137, 1872–1875.

(12) Xu, J. T.; Zhou, J. J.; Chen, Y. H.; Yang, P. P.; Lin, J. Lanthanide-activated nanoconstructs for optical multiplexing. *Coord.Chem. Rev*. **2020**, 415, 213328–213345.

(13) Gorris, H. H.; Wolfbeis, O. S. Photon-upconverting nanoparticles for optical encoding and multiplexing of cells, biomolecules, and microspheres. *Angew. Chem. Int. Ed*. **2013**, 52, 3584–3600.

(14) Huang, K.; Idris, N. M.; Zhang, Y. Engineering of lanthanide-doped upconversion nanoparticles for optical encoding. *Small*. **2016**, 12, 836–852.

(15) Richardson, F. S. Terbium(III) and europium(III) ions as luminescent probes and stains for biomolecular systems. *Chem. Rev*, **1982**, 82, 541–552.

(16) Zhou, L. J.; Deng, W. H.; Wang, Y. L.; Xu, G.; Yin, S. G.; Liu, Q. Y. Lanthanide-potassium biphenyl-3,3'-disulfonyl-4,4'-dicarboxylate frameworks: gas sorption, proton conductivity, and luminescent sensing of metal Ions. *Inorg. Chem*. **2016**, 55, 6271–6277.

(17) Li, Y. J.; Wang, Y. L.; Liu, Q. Y. The highly connected MOFs constructed from nonanuclear and trinuclear lanthanide-carboxylate clusters: selective gas adsorption and luminescent pH sensing. *Inorg. Chem*. **2017**, 56, 2159–2164.

(18) Lee, T.; Lee, H. L.; Tsai, M. H.; Cheng, S. L.; Lee, S. W.; Hu, J. C.; Chen, L. T. A biomimetic tongue by photoluminescent metal-organic frameworks. *Biosens. Bioelectron*. **2013**, 43, 56–52.

(19) Yang, W. T.; Bai, Z. Q.; Shi, W. Q.; Yuan, L, Y.; Tian, T.; Chai, Z. F.; Wang, H.; Sun, Z. M. MOF-76: from a luminescent probe to highly efficient U^{VI} sorption material. *Chem. Commun*. **2013**, 49, 10415–10417.

(20) Zhang, H. J.; Fan, R. Q.; Wang, P.; Wang, X. M.; Chen, W.; Zheng, X. B.; Li, K.; Yang, Y. L. Crystal structures and effect of temperature on the luminescence of two lanthanide coordination polymers with twofold interpenetrating pcu topology. *J. Inorg. Organomet. Polym.* **2014**, 24, 624–632.

(21) He, H.; Ma, H.; Sun, D.; Zhang, L.; Wang, R.; Sun, D. Porous lanthanide-organic frameworks: control over interpenetration, gas adsorption, and catalyst properties. *Cryst. Growth Des.* **2013**, 13, 3154–3161.

(22) Reineke, T. M.; Eddaoudi, M.; Fehr, M.; Kelley, D.; Yaghi, O. M. From condensed lanthanide coordination solids to microporous frameworks having accessible metal sites. *J. Am. Chem. Soc*. **1999**, 121, 1651–1657.

(23) Rieter, W. J.; Taylor, K. M. L.; An, H. Y.; Lin, W. L; Lin, W. B. Nanoscale metal-organic frameworks as potential multimodal contrast enhancing agents. *J. Am. Chem. Soc*. **2006**, 128, 9024–9025.

(24) Hatakeyama, W.; Sanchez, T. J.; Rowe, M. D.; Serkova, N. J.; Liberatore, M. W.; Boyes, S. G. Synthesis of Gadolinium nanoscale metal-organic framework with hydrotropes: manipulation of particle size and magnetic resonance imaging capability. *ACS Appl. Mater. Interfaces* **2011**, 3, 1502–1510.

(25) Zhang, H. J.; Fan, R. Q.; Wang, P.; Wang, X. M.; Chen, W.; Zheng, X. B.; Li, K.; Yang, Y. L. Crystal structures and effect of temperature on the luminescence of two lanthanide coordination polymers with twofold interpenetrating pcu topology. *J. Inorg. Organomet. Polym.* **2014**, 24, 624–632.

(26) He, H.; Ma, H.; Sun, D.; Zhang, L.; Wang, R.; Sun, D. Porous lanthanide-organic frameworks: control over interpenetration, gas adsorption, and catalyst properties. *Cryst. Growth Des.* **2013**, 13, 3154–3161.

(27) *CrysAlisPro*; Rigaku Oxford Diffraction: The Woodlands, TX **2015**.

(28) Sheldrick, G. M. Crystal structure refinement with SHELXL. *Acta Crystallogr., Sect. C: Struct. Chem*. **2015**, C71, 3−8.

(29) Chakraborty, G.; Mandal, S. K. Neutral luminescent metal-organic frameworks: structural diversification, photophysical properties, and sensing applications. *Inorg. Chem.* **2017**, 56, 14556–14566.